Build Simul (2023) 16: 2093–2107
https://doi.org/10.1007/s12273-023-1051-z

A newly designed BIPV system with enhanced passive cooling and ventilation

Hadi Ahmadi Moghaddam (✉), Svetlana Tkachenko, Guan Heng Yeoh, Victoria Timchenko

School of Mechanical and Manufacturing Engineering, University of New South Wales, Sydney, NSW 2052, Australia

Abstract

Nowadays, the application of renewable energies such as solar energy in the building sector has increased notably considering the adverse impacts of climate change on human life; hence many studies have focused on the application of photovoltaic panels in buildings. In the current study, a 3D computational fluid dynamics (CFD) model has been developed to evaluate the performance of a newly designed building-integrated photovoltaic (BIPV) system. Given the negative influence of overheating on the lifespan and performance of PV panels, their passive air cooling has been studied. Further, the potential of rooftop-mounted solar panels in passive ventilation of buildings by generating natural convective currents has been explored. The developed CFD model takes into consideration the effects of radiation, conduction, and buoyancy-driven natural convective currents generated by solar PV panels which are heated due to the exposure to solar radiation heat flux. The results suggest that applying a high surface emissivity for the part of the roof beneath the PV panels intensifies the natural convective currents which in turn provides better cooling for PV panels with higher cooling effects at higher solar heat fluxes. Up to a 34% increase in the convective mass flow rate and a 3 K decrease in the mean temperature of the panels were attained by modifying the emissivity of roof surface. Such a 3 K decrease in the operating temperature of the PV panels can enhance their efficiency and lifespan by about 1.56% and 21%, respectively. Based on the operating conditions and system characteristics, the BIPV system yielded an air change rate (ACH) in the range of 3–13 which was considered to be highly prevalent in providing the required passive ventilation for a wide range of applications. It was also observed that the flow dynamics inside the building were affected by both the amount of solar heat load incident on the solar panels and the emissivity of the roof surface behind the panels.

Keywords

air change rate
BIPV
natural convection
passive cooling
passive ventilation
surface emissivity

Article History

Received: 12 April 2023
Revised: 10 May 2023
Accepted: 27 May 2023

1 Introduction

Buildings are considered a major energy consumer as they consume about 36% of the global energy and 55% of global electricity making them responsible for about 40% of the overall carbon dioxide emissions, thereby intensifying global warming implications (Maghrabie et al. 2021). On the other hand, within buildings, the share of HVAC systems in energy usage which is within the range of 40% to 60% highlights the necessity of utilizing renewable energy resources such as solar, wind, or geothermal energy in buildings considering the adverse environmental impacts of using fossil fuels for electricity generation (Orme 2001; Pérez-Lombard et al. 2008; Sartori et al. 2012; Zhang et al. 2021; Ahmed et al. 2022).

The application of photovoltaic (PV) modules, which convert solar radiation into electricity, in buildings has received significant attention in recent years. Generally, these panels are added to the structure of a building in the form of a façade-mounted design or rooftop-mounted design, the latter case being the widespread adopted design (Shukla et al. 2017). Further, these systems can be classified as building-applied photovoltaic (BAPV) or building-integrated photovoltaic (BIPV). In a BAPV system, the PV modules are placed on the building's surface or roof (usually with a gap between the panels and surface to allow passive

E-mail: h.ahmadi_moghaddam_dastjerdi@unsw.edu.au

List of symbols

ACH	air change rate per hour
BAPV	building-applied Photovoltaic
BIPV	building-integrated Photovoltaic
CFD	computational fluid dynamics
C_p	specific heat [J/(kg·K)]
g	gravitational acceleration [m/s^2]
k	thermal conductivity [W/(m·K)]
PCM	phase change material
PV	photovoltaic
q	heat flux applied on solar cells [W/m^2]
Q	volumetric flow rate [m^3/s]
Ra	Rayleigh number
T	temperature [K]
u	velocity [m/s]
α	thermal diffusivity [m^2/s]
β	thermal expansion coefficient [K^{-1}]
ε	emissivity
η	efficiency of PV panels
ν	kinematic viscosity [m^2/s]
ρ	density [kg/m^3]
σ	Stefan-Boltzmann constant [W/(m^2·K)]

Subscripts

i, j	generic space coordinates
amb	ambient
STC	standard test condition

cooling of panels from the backside); while in a BIPV system, the modules are considered as a part of the building structure (Singh et al. 2021).

One of the challenges of using PV modules is that the electrical efficiency and lifespan of PV panels degrade with a rise in their temperature due to the exposure to solar radiation. To tackle this issue, different cooling techniques have been proposed and assessed. Generally, cooling or thermal management techniques can be classified as active and passive. In active techniques, external mechanical devices such as pumps or fans are required to recirculate the coolant and cool down the PVs. Previous investigations have evaluated the thermal management of PVs by water cooling (Daghigh et al. 2011; Prudhvi and Sai 2012), water spray cooling (Moharram et al. 2013; Elnozahy et al. 2015), forced convective cooling by air (Sajjad et al. 2019; Maghrabie et al. 2020), or the combination of air and water forced convective cooling (Kabeel et al. 2019). Although, the cooling potential of active techniques may be greater than passive techniques, their application in BIPV/BAPV systems has remained limited as they require external power and mechanical devices for cooling which is accompanied by further energy consumption, maintenance costs, and noise. The studies conducted on the cooling of PV panels by active methods were limited to lab-scale cases, and their application and functionality in real-scale BIPV/BAPV systems are rarely evaluated.

Contrary to active methods, passive methods do not need an external power source or mechanical devices for cooling purposes leading to lower costs and fewer maintenance needs. Regarding the passive cooling, phase change material (PCM) (Salem et al. 2019; Karthick et al. 2020), heat pipe (Habeeb et al. 2017; Alizadeh et al. 2018), heat sink (Firoozzadeh et al. 2019; Arifin et al. 2020; Parkunam et al. 2020), radiative cooling (Sun et al. 2017; An et al. 2019), and natural (free) convection (Lau et al. 2012a) are widely studied techniques. Some issues associated with PCMs such as corrosion (Dwivedi et al. 2020) or high costs (Asefi et al. 2021) impede their widespread usage in the building sector. Regarding heat pipes, their usage in BIPV systems on a large scale could be challenging due to their structure that requires a sealed system comprising high thermally conductive pipes at both ends, i.e., condenser and evaporator. It has also been reported that the cooling performance of these systems may degrade due to the large thermal contact resistance between the PV panels and heat pipes (Dwivedi et al. 2020). However, natural convection by air alone or combined with heat sinks is an interesting method for BIPV systems. Passive air cooling is simple and can be applied for real scale BIPV systems. Air is free and accessible, and in addition to the thermal management purposes, it can be used for ventilation purposes as well, as will be discussed in the following.

A schematic view of a PV panel installed on the surface of a building is shown in Figure 1. As observed, a gap between the two surfaces has been considered through which air can pass. When the PV panel experiences high temperatures due to exposure to solar radiation, buoyant forces are generated resulting in natural or free convective currents. This natural convective flow has a considerable passive cooling impact. In this regard, Ritzen et al. (2017) conducted experiments on lab scale PVs with different volumes of backward ventilation. They monitored the system performance and found out that after three years, the efficiency of the non-ventilated PVs had dropped by 86%. Their experiments demonstrated that the maximum temperature experienced by non-ventilated PVs was 11 °C over the ventilated PVs. Within another experimental and

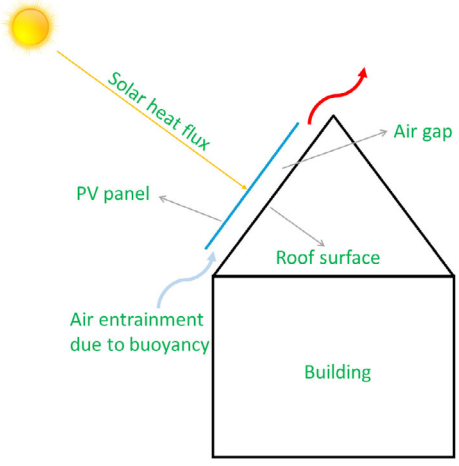

Fig. 1 Schematic view of a building-applied PV (BAPV) system

numerical research on double-skin façade BIPV, Lai and Hokoi (2017) observed that under identical heat fluxes, the electrical output of ventilated PVs was 16% to 44% over that of the non-ventilated PVs in which the panels were directly installed on surface of the wall without a gap between them. Gan (2009) developed a CFD model and explored the role of gap size between the PV and wall. The numerical results suggested that adequate air gap behind the PV panel is required to allow the air to flow and avoid overheating and prevalence of hot spots on the panel. Depending on the inclination angle and length of the panels, a gap size in the range of 10 to 16 cm was proposed. Another CFD simulation conducted by Lau et al. (2020) suggested an optimum air gap between 10 and 12.5 cm for reaching low temperatures in PV. Similar observations regarding the role of gap size on vertically installed PVs were reported in other experiments (Agathokleous and Kalogirou 2018a, 2018b). In addition to gap size, the effects of other parameters such as heat flux, heating mode, gap aspect ratio, wind, solar radiation, or the inclination angle of the PVs have been assessed in other investigations (Lau et al. 2012a; Lau et al. 2012b; Brandl et al. 2014; Li et al. 2015; Tkachenko et al. 2016; Zhang et al. 2020). Lau et al. (2012a) through Large Eddy Simulation (LES) models reported that the vertical channel with smaller width exhibits different turbulent quantities, thereby affecting the heat transfer rates. Another numerical study by Lau et al. (2012b) showed that for both titled and vertical channel configurations, the staggered heating mode enhanced the cooling rate and convective mass flow rate. A study by Zhang et al. (2020) highlighted that the incidence angle and the velocity of wind currents are among the influencing factors in the cooling of solar panels in buildings. Another CFD study by Brandl et al. (2014) showed that the opening of the façade affects the flow dynamics within the channel, thereby modifying the heat removal from the walls.

It is worth noting that the above-mentioned studies have solely investigated the passive cooling of PVs whether in real-scales or lab-scales, but the channel or gap behind the PVs was not integrated into the interior of buildings representing a BAPV system (see Figure 1). In addition to the primary function of the generated natural convective flow behind the panels i.e., passive cooling of PV modules, it could be possible to utilize this current for passive ventilation of buildings through chimney effects by integrating the gap behind the PVs into the interior of the buildings. A schematic view of the proposed BIPV system is shown in Figure 2. As seen, the gap between the PV modules and roof has been integrated into the interior of the building, and due to the formation of buoyant flows behind the panels in the gap, the fresh air is entrained into the room through window.

Passive ventilation, as an energy-efficient method for decreasing building energy usage, has been found to be effective in providing adequate indoor air quality without electricity demand whose elements include airflow rate, air change rate, etc., thereby improving the thermal comfort of the residents (Jomehzadeh et al. 2017). The idea of using chimney effects in large scales or small scales for passive ventilation of buildings is not novel and has been studied thoroughly (Bansal et al. 1993; Mathur and Mathur 2006; Khanal and Lei 2011; Rabani et al. 2014; Moosavi et al. 2020; Zhang et al. 2021). Generally, one idea in these studies on solar chimneys is to augment the solar gain, thereby establishing an adequate temperature difference between the inside and outside of the structure in order to drive a sufficient fresh airflow rate. However, the idea of using PV panels for passive ventilation of buildings in BIPV systems is rarely studied. There are limited studies evaluating the ventilation of buildings equipped with PV panels alone or in combination with a solar chimney installed on the roof or façade (Khedari et al. 2002; DeBlois et al. 2013; Tkachenko et al. 2021). Using a BIPV system for passive ventilation of buildings could be more beneficial than a solar chimney as

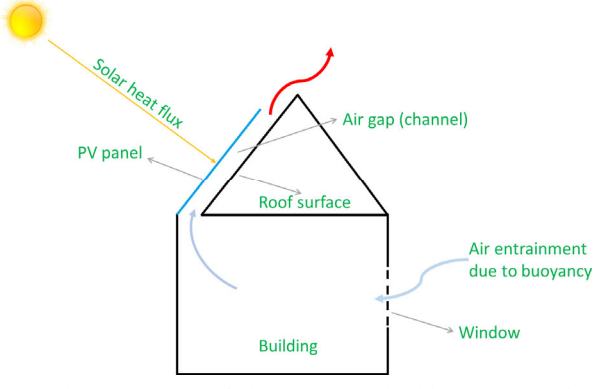

Fig. 2 Schematic view of the proposed building-integrated PV (BIPV) system

the BIPV system also offers the opportunity to generate electricity from solar energy as a clean energy resource while a solar chimney system solely provides ventilation. The current research aims at modelling natural convective currents in BIPV systems in real scales. For this purpose, a 3D CFD model has been developed to simulate a one storey building with rooftop-mounted PVs. CFD is found to be capable of accurately predicting flow patterns, velocity and temperature profiles, and other characteristics of fluid flows in building applications (Khanal and Lei 2011); while the experimental study of buildings generally can be more challenging because of their large size. Also, the experimental study of buildings are expensive and inefficient to modify the structure layout (Park and Battaglia 2015).

Therefore, this study numerically explores two aspects none of which, to the best knowledge of authors, have been investigated previously:

- The potential of PV panels in passive ventilation of a building in real scales due to the natural convective flows generated by panels: There is no previous study to evaluate the capability of PV panels in passive ventilation of buildings.
- The impacts of surface emissivity for the part of the roof beneath the PV panels on the cooling of PV panels and ventilation rate of the building's interior: There is no previous study to illustrate the role of roof surface emissivity on the enhancement of passive cooling of PV panels.

In the following sections, the proposed BIPV system and the numerical setup are described. Then, the results are presented and discussed after validation of the numerical model against benchmark experimental data from the literature.

2 Case study description

The studied geometry, as shown in Figure 3, is a one storey building with PV panels installed on top of its slanted roof. The gap or channel between the PV panels and the roof is sealed from sides to avoid either flow entering/leaving the channel from/to outside environment. However, there is an opening at the end of the channel from which the naturally generated flow due to buoyancy effects can pass and leave the channel. The channel is integrated into the interior of the building for passive ventilation purposes. The dimensions of the structure are H = 1608 mm, $L1/H$ = 1.87, $L2/L1$ = 1.89, $L3/L1$ = 1.33. The building includes an opening or window with sides $L4 = 2 \times L5 = L1$. A relatively large size window has been chosen in this study as it is common to use large windows in Australian buildings. The inclination angle of the PV panels and roof is 45° (Zhai et al. 2005). The size of the gap between the panels and roof surface is $L6$ = 150 mm (Gan 2009). It is assumed that the surface of the roof in channel and sides of the channel are covered with a 5 mm aluminum sheet and insulated to avoid heat loss to the surrounding and maximize the buoyancy effects. Moreover, it is assumed that the ceiling and floor of the building are insulated (Rabani et al. 2014).

The panels are comprised of five layers including glass cover, EVA, PV cell, EVA, and Tedlar, respectively; Tedlar being the layer adjacent to the channel and glass cover adjacent to the external environment. More information of the dimensions of the panels and the thermophysical properties of the components is provided in Table 1 (Zhou et al. 2022). The emissivity of Tedlar and glass is assumed to be 0.84 (Zhou et al. 2021). The thermal conductivity, density, and heat capacity of brick (used in walls) are 0.73 W/(m·K), 1700 kg/m^3, and 800 J/(kg·K), respectively. Moreover, the thermal conductivity, density, and heat capacity of aluminum are 202 W/(m·K), 2719 kg/m^3, and 871 J/(kg·K), respectively.

In this research, to compare the performance of the BAPV and BIPV systems under different environmental conditions, two different values of 293 and 303 K for ambient temperature and three different values of 200, 500,

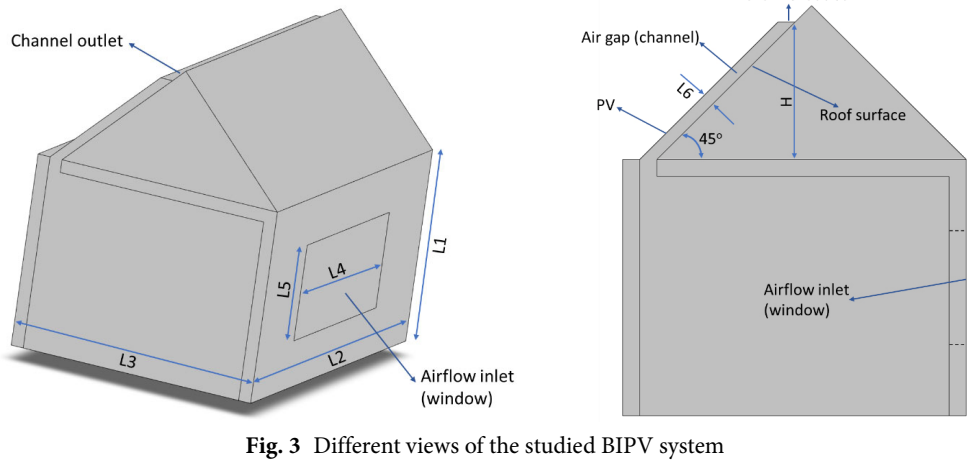

Fig. 3 Different views of the studied BIPV system

Table 1 Characteristics of the PV panels

Component	Thickness [m]	Thermal conductivity [W/(m·K)]	Density [kg/m^3]	Specific heat [J/(kg·K)]
Glass	3000×10^{-6}	1.8	3000	500
EVA	500×10^{-6}	0.35	960	2090
Silicon	175×10^{-6}	130	2329	700
Tedlar	100×10^{-6}	0.2	1200	1250

and 800 W/m^2 for heat flux (q) applied on the solar cells are considered corresponding to the Ra numbers in the range of 6.3×10^{12} to 25.9×10^{12}. The Ra number is computed according to Eq. (1) (Beji et al. 2017):

$$Ra = \frac{g\beta q H^4}{\alpha \nu k} \tag{1}$$

where g, β, q, H, α, ν and k represent the gravitational acceleration [m/s^2], thermal expansion coefficient [K^{-1}], heat flux applied on solar cells [W/m^2], channel height [m], thermal diffusivity [m^2/s], kinematic viscosity [m^2/s], and thermal conductivity of air [W/(m·K)], respectively.

It is worth noting that of total solar radiation incident on a PV panel, a portion is reflected and converted into electricity, and the rest is transformed into heat thereby increasing the temperature of the module. The heat fluxes used here are considered to be the heat applied on the cells which increases their temperature.

To reveal the role of roof surface emissivity (ε), two different values of 0.2 and 0.9 are considered for the surface of the roof adjacent to the channel which is achievable through applying low/high emissive coatings. Different cases studied here are listed in Table 2.

Table 2 Different cases studied in this research

Case	Heat flux (q) [W/m^2]	Ambient temperature [K]	Roof surface emissivity (ε)
1	800	303	0.9
2	800	303	0.2
3	500	303	0.9
4	500	303	0.2
5	200	303	0.9
6	200	303	0.2
7	800	293	0.9
8	500	293	0.9

3 Numerical setup

Ansys Fluent (ANSYS 2021) CFD package is used for 3D simulation of the BIPV system. Unsteady Reynolds Averaged Navier-Stokes (URANS) approach is employed to obtain the thermal-fluid fields of the system by solving the mass, momentum, and energy conservation equations, as presented by Eqs. (2)–(4), respectively:

$$\frac{\partial \rho}{\partial t} + \frac{\partial (\rho u_j)}{\partial x_j} = 0 \tag{2}$$

$$\frac{\partial (\rho u_i)}{\partial t} + \frac{\partial (\rho u_i u_j)}{\partial x_j} = -\frac{\partial p}{\partial x_i} + \frac{\partial \sigma_{ij}}{\partial x_j} + (\rho - \rho_{\text{ref}}) g_i \tag{3}$$

$$\frac{C_p \partial (\rho T)}{\partial t} + \frac{C_p \partial (\rho u_i T)}{\partial x_j} = k \frac{\partial}{\partial x_j}\left(\frac{\partial T}{\partial x_j}\right) + \frac{\partial q_j}{\partial x_j} \tag{4}$$

The Shear Stress Transport (k-ω SST) model developed by Menter (1994) is used to model the natural convective flow. This model is found to be capable of predicting the flow features in natural convective flows with reasonable accuracy (Wu and Lei 2015) while its computational costs is much less than other expensive approaches such as Large Eddy Simulation (LES) or Direct Numerical Simulation (DNS). The SST model is a hybrid model that uses k-ω formulation inside the boundary layer and then switches to k-ε formulation in the areas outside the boundary layer making it suitable for many industrial and engineering applications (Moghaddam et al. 2019; ANSYS 2021). The following transport equations have been used to obtain the turbulent kinetic energy (k) and specific dissipation rate (ω):

$$\frac{\partial}{\partial t}(\rho k) + \frac{\partial}{\partial x_i}(\rho k u_i) = \frac{\partial}{\partial x_j}\left(\Gamma_k \frac{\partial k}{\partial x_j}\right) + G_k - Y_k + S_k + G_b \tag{5}$$

$$\frac{\partial}{\partial t}(\rho \omega) + \frac{\partial}{\partial x_i}(\rho \omega u_i) = \frac{\partial}{\partial x_j}\left(\Gamma_\omega \frac{\partial \omega}{\partial x_j}\right) + G_\omega - Y_\omega + D_\omega + S_\omega + G_{\omega b} \tag{6}$$

In the above equations, G_k and G_ω represent the production of turbulent kinetic energy and generation of ω, respectively. Γ_k and Γ_ω show the effective diffusivity of k and ω, respectively. S_k and S_ω represent user-defined source terms. D_ω illustrates the cross-diffusion term. Y_k and Y_ω show the dissipation of k and ω because of turbulence. G_b and $G_{\omega b}$ show the buoyancy terms. Further details of the transport equations can be found in Ansys Fluent Theory Guide (2021).

A structured mesh is adopted for the flow domain

inside the room and channel, but an unstructured mesh is utilized for the external domain. To ensure that the numerical results are mesh-independent, different meshes with cell numbers from 9.1 M to 16.8 M were tested. As observed in Figure 4, the mesh density has slight impacts on the obtained results including the mean temperature of the PV panels and the natural convective mass flow rate. The maximum relative difference between the current mesh (13.9 M cells) with the finer mesh (16.8 M cells) was below 0.5% for both the mean temperature of PV panels and mass flux. Therefore, using the mesh with 13.9 cells was justified to avoid excessive costs. Different views of the BIPV system inside the external domain, the structured mesh used in the room and channel, and the unstructured mesh used in the external domain are illustrated in Figure 5. Generally, the mesh density is higher in the areas where a sharp gradient of temperature or velocity is anticipated. An external cylindrical domain with the height of 24 m and diameter of 38 m is modelled to accurately capture flow entrainment into the building and decrease the effects of boundary conditions on the numerical solution (Park and Battaglia 2015). Moreover, as the temperature of PV is a strong function of convective and radiative heat transfer to the surrounding environment, it was required to include an external domain to model these heat transfer mechanisms; or in the case of building without an external domain, it was required to use empirical correlations to account for the heat transfer coefficient between the panels and environment. However, our initial assessments showed that there is not such a reliable correlation for this scenario. So, the external domain was included in the model to consider the convective cooling from PV's outer surface exposed to the ambient.

The time step in the present transient model was 0.05 sec. Using a smaller time step did not yield a sensible change in results including the temperature of PV or convective mass flow rate but increased the computational expenses; however, using larger time steps imposed instabilities and convergence problems in some cases of the numerical simulations. In addition to the mesh and time step size, a sensitivity analysis for the type of turbulence model was also conducted to show the extent to which the obtained numerical data were affected by these models. In this regard, two other frequently-used RANS models including k-ε realizable and k-ε RNG are tested for only Case 1 and Case 8 in Table 2 to avoid excessive computational costs. The obtained results for mean mass flow rate and mean temperature of PV showed that the maximum difference between the different turbulence models was below 6%.

It should be mentioned that to reduce the computational costs, primarily the steady RANS technique was used, but tracking the flow features such as mass flow rate and PV temperature showed that the flow physics was unsteady in nature and required a transient model, therefore URANS was used. But, to analyze and compare the results, all data and contours presented in this research have been averaged over 15 minutes of flow time.

To model the radiation effects, the surface-to-surface radiation model has been used which assumes the surfaces to be diffuse and gray. The energy reflected from a given surface (n) is computed according to the following equation:

$$q_{\text{out},n} = \rho_n q_{\text{in},n} + \varepsilon_n \sigma T_n^4 \tag{7}$$

In Eq. (7), terms $q_{\text{out},n}$, σ, ε_n, and $q_{\text{in},n}$ show the energy flux leaving surface n, Stefan-Boltzmann constant, emissivity of surface n, and energy flux incident on the surface n from

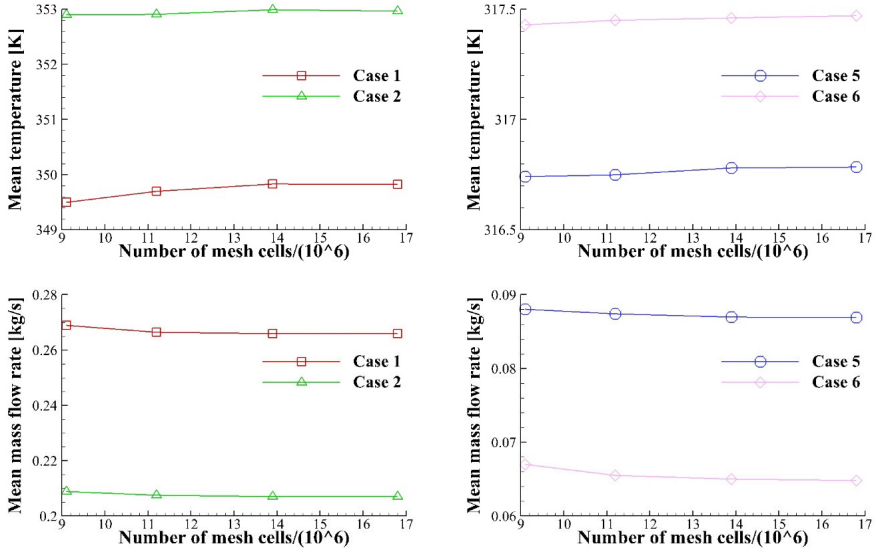

Fig. 4 Effects of the mesh density on the numerical solution under different cases

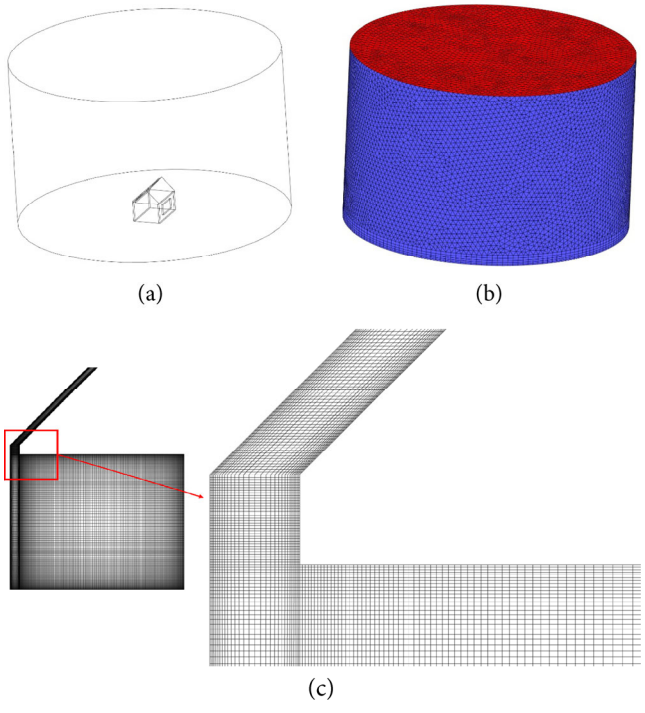

Fig. 5 (a) A 3D view of the external domain and building, (b) a 3D view of the unstructured mesh used in the external domain, (c) a side view of the structured mesh used in the room and channel

the surroundings, respectively. Further, $\rho_n = 1 - \varepsilon_n$ is the reflectivity of surface n. The amount of energy incident on the surface from other surfaces is directly dependent on the surface-to-surface view factor which is calculated and stored in Fluent.

To account for the radiation heat transfer from the PV panels to sky, sky temperature is calculated according to (Swinbank 1963; Evangelisti et al. 2019):

$$T_{\text{sky}} = 0.0552 \times T_{\text{amb}}^{1.5} \tag{8}$$

where T_{amb} is the ambient temperature.

4 Results and discussion

4.1 Validation of the CFD model

The empirical benchmark data for turbulent natural convection of air inside a square cavity reported by Tian and Karayiannis (2000) and Ampofo and Karayiannis (2003) is considered for validation of the present numerical model. As shown in Figure 6, the test rig was a square cavity with dimensions $L = H = 0.5D = 750$ mm. The vertical hot and cold walls made from mild steel with a thickness of 6 mm were kept at constant temperatures of 323 K and 283 K, respectively while the horizontal top and bottom walls made from 1.5 mm mild steel (with wood and polystyrene layers attached) were conducting walls resulting

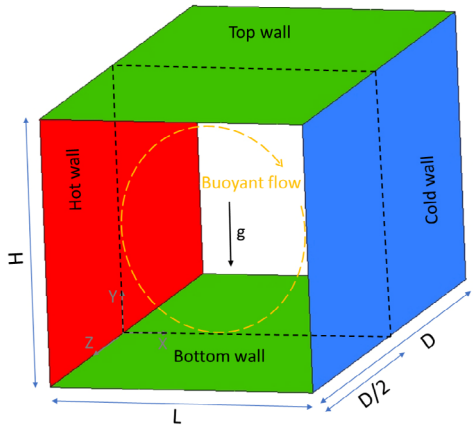

Fig. 6 Schematic view of the test cavity

in a turbulent natural convective flow with Ra number of 1.58×10^9. The test room temperature was kept at 303 K equal to the mean temperature of hot and cold walls. The temperature and velocity measurements were made at the cavity center plane (shown by the dashed line) at different heights. Further details of the experimental test rig and measurement methods can be found in Tian and Karayiannis (2000) and Ampofo and Karayiannis (2003). The main heat and mass transfer mechanisms of this experiment are similar to those of the current numerical research including natural convection, conduction, and radiation, making it a suitable reference for the validation of the current CFD model. There is conduction heat transfer through the horizontal top and bottom conducting walls (comprised of three layers including steel, wood, and polystyrene) in the experimental cavity and in the PV panel (comprised of glass, EVA, Silicon, and Tedlar) in the current model. The validity of the shell conduction model to simulate the conduction heat transfer was obtained during the validation against this experimental work and then was applied in modelling conduction in PV panels. There is natural convection in both systems. However, the natural convection in the cavity is triggered by the hot and cold walls with constant temperatures. The constant temperature walls were achieved by means of temperature control apparatus which maintained a constant-temperature water flow to two chambers connected to the hot and cold walls. But, in the current model, the PV panel with constant heat flux triggers the buoyant forces. The constant heat flux applied on the panels represents the portion of the incident solar radiation heat flux which is turned into heat within the panel.

A comparison of the experimental and numerical velocity and temperature measurements in the cavity center at different heights near the hot and cold walls where the flow experiences higher activity is presented in Figures 7 and 8. It is observed that the numerical model reasonably predicts the experimental velocity and temperature measurements

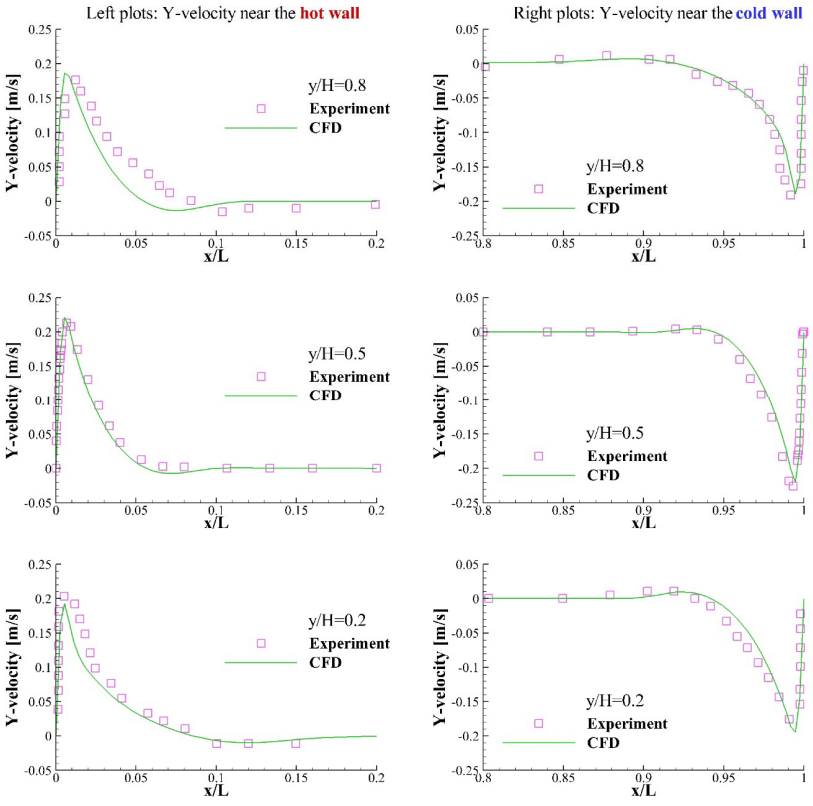

Fig. 7 Comparison of the experimental (Tian and Karayiannis 2000; Ampofo and Karayiannis 2003) and numerical measurements for *Y*-velocity at different locations inside the cavity

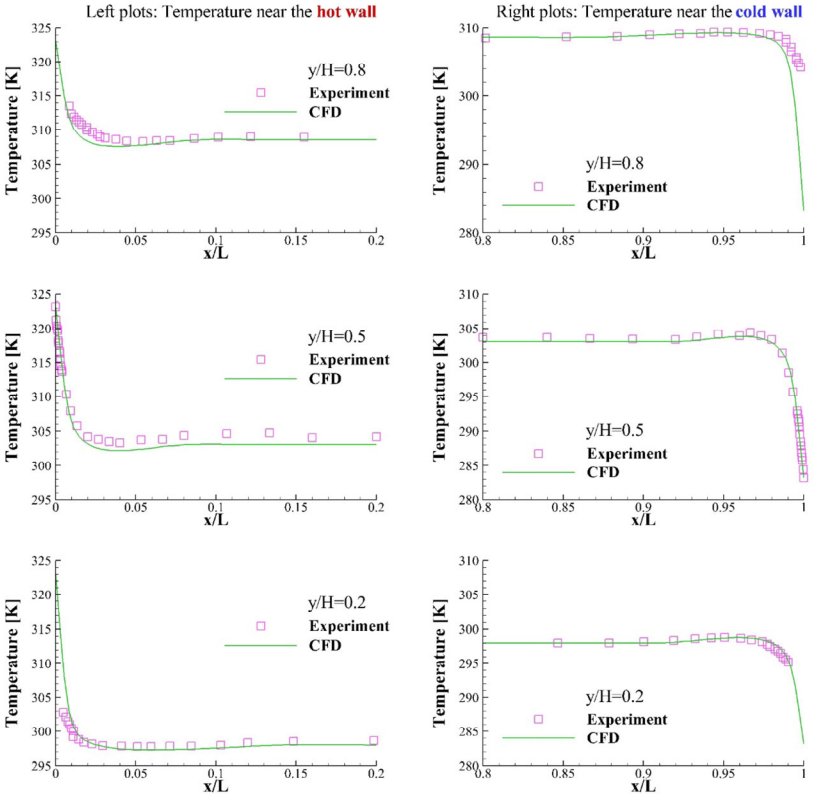

Fig. 8 Comparison of the experimental (Tian and Karayiannis 2000; Ampofo and Karayiannis 2003) and numerical measurements for temperature at different locations inside the cavity

at different locations. It should be noted that the authors were not able to extract the experimental temperature data very close to the hot and cold walls at $y/H = 0.2$ and $y/H = 0.8$ as the relevant plots were not clear and readable in these areas. However, it is seen that the temperature readings have been predicted with reasonable accuracy in other locations where the experimental temperature data were available. Also, for $y/H = 0.5$ where the temperature data were available very close to the hot and cold walls, it is seen that the numerical model predicts the experimental data reasonably well. The maximum difference between the peak of Y-velocity obtained experimentally and numerically is about 12%, and the maximum difference between the experimental and numerical temperature measurements is below 1%.

4.2 BIPV vs BAPV

As this research proposes a new design to move from BAPV to BIPV and to ensure that the proposed system will not adversely affect the performance of the PV modules, it is necessary to first evaluate and compare the performance of both systems in terms of operating temperatures that the modules in both systems will experience under identical conditions. The structure in both systems is identical except that in the BIPV system, the gap behind the modules has been sealed from the surroundings and integrated into the interior of the building (for passive ventilation purposes) while in the BAPV system the gap behind the PV panels is open to the surrounding (schematically shown in Figures 1 and 2). The temperature contours averaged through the PV panel thickness in both systems are shown in Figure 9 for the heat flux of 800 W/m^2 and ambient temperature of 303 K (Case 1). It is seen that in the BAPV system, the sides of the panels experience lower temperatures as compared to the core areas as air can be entrained into the gap from the sides. However, in the BIPV system, the lower edge of the modules experiences lower temperatures due to direct contact with the air entering the channel from the building. Similar observations are made under other ambient conditions. As shown in Table 3, the average operating temperatures and maximum temperature of the modules in the BAPV and BIPV systems under identical conditions do not show big differences suggesting that the proposed BIPV system under natural convection mechanism has no adverse impact on the operating temperatures of the modules as compared to the counterpart BAPV system. To avoid excessive computational costs only four cases which include different operating conditions were selected to compare the performance of BIPV and BAPV systems.

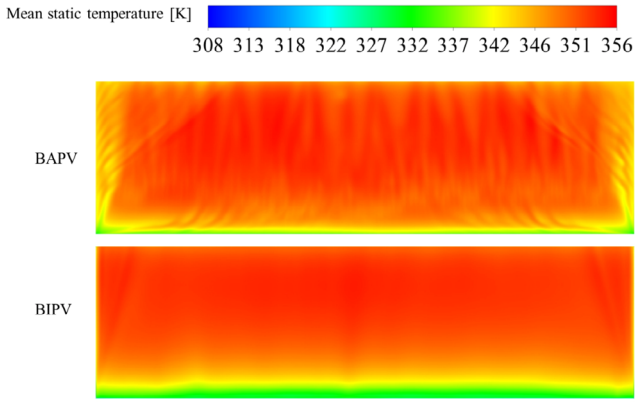

Fig. 9 Contours of temperature of PV panels in BIPV and BAPV for Case 1

4.3 Thermal-fluid characteristics of the BIPV system

In this section, the impacts of heat flux and surface emissivity of the roof behind the modules on the cooling of panels, passive ventilation rate, and flow physics have been explored.

The variations of free convective mass flow rate and mean temperature of the panels with heat flux and roof surface emissivity are presented for different cases in Table 4. However, to better interpret the results, plots in Figure 10 are presented. It is observed that, as expected, the mass flow rate is higher as the heat flux rises due to the intensified buoyancy effects. To reveal the effects of solar heat flux on flow physics, the contours of velocity vectors under different heat fluxes have been shown in Figure 11 for Case 1 and Case 3. It is seen that, due to the higher momentum of the flow entering the room at higher heat flux, the inflow travels a longer path and touches the floor in the middle of the room resulting in the formation of a vortex in the bottom right corner of the room larger than that of the lower heat flux. In the case of low heat flux, the flow entering the room from the window has lower momentum, therefore touches the floor earlier. It is seen that the amount of solar heat flux affects the flow structure inside the building.

It is also observed in Figure 10 that increasing the roof surface emissivity augments the convective mass flow rate which in turn decreases the mean temperature of the PV

Table 3 Comparison of the mean temperature of PV panels in BIPV and BAPV configurations under identical conditions

Case	Mean temperature of PV in BAPV [K]	Maximum temperature of PV in BAPV [K]	Mean temperature of PV in BIPV [K]	Maximum temperature of PV in BIPV [K]
1	351	356	350	355
3	335	338	334	338
7	344	350	344	349
8	330	333	329	332

Table 4 Variations of mean temperature of PV panels and natural convective mass flow rate under different conditions

Case	Mean temperature of panels [K]	Mass flow rate [kg/s]
1	350	0.266
2	353	0.207
3	334	0.184
4	336	0.151
5	317	0.087
6	318	0.065
7	344	0.306
8	329	0.225

modules. The reason behind this effect is that by increasing the surface emissivity, the temperature of the roof surface augments, and the roof acts as a heated surface giving rise to buoyant flows. Therefore, the convective mass flow rate and PV cooling rate augment. At heat fluxes of 800, 500, and 200 W/m^2, the increase in the mass flow rate by increasing the roof surface emissivity is about 29%, 22%, and 34%. Correspondingly, the mean temperature drop of panels at these heat fluxes is about 3 K, 2 K, and 1K respectively suggesting that applying roof with high surface emissivity for PV cooling at higher heat fluxes is more effective than that at lower heat fluxes. When the heat flux incident on the panels is high, the increase in the temperature of the roof surface due to enhanced emissivity is noticeable. Therefore, the change in the free convective flow rate and cooling rate of panels is higher. However, at lower heat fluxes, the change in the temperature of the roof surface due to the change in its surface emissivity is low, consequently, the change in the free convective flow and cooling rates is lower.

The velocity contours inside the channel on the center plane are shown for the heat flux of 800 W/m^2 and roof surface emissivity of 0.9 and 0.2 (Case 1 and Case 2) in Figure 12. When the emissivity of the roof surface is low, the air entrainment into the channel occurs due to buoyancy force in the vicinity of the hot PV panel. Buoyant forces generated in the boundary layer adjacent to the hot PV panel result in the upward movement of airflow inside the channel and air entrainment into the channel from the bottom, but the cold roof surface does not contribute to the buoyant flow generation. But, when the emissivity of the roof surface is increased, its temperature increases as well. In this scenario, it acts like a heated surface and similar to the PV panel contributes to the formation of buoyant currents. Therefore, when the roof surface emissivity is high, the natural convective mass flow rate is higher as both surfaces simultaneously contribute to the air entrainment into the channel thereby decreasing the panel temperature due to enhanced convective and radiative cooling effects and enhancing the ventilation rate of the building's interior. This can be deduced by comparing the velocity distribution near

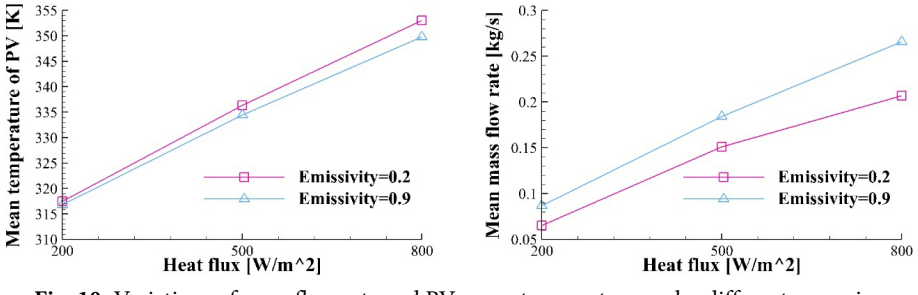

Fig. 10 Variations of mass flow rate and PV mean temperature under different scenarios

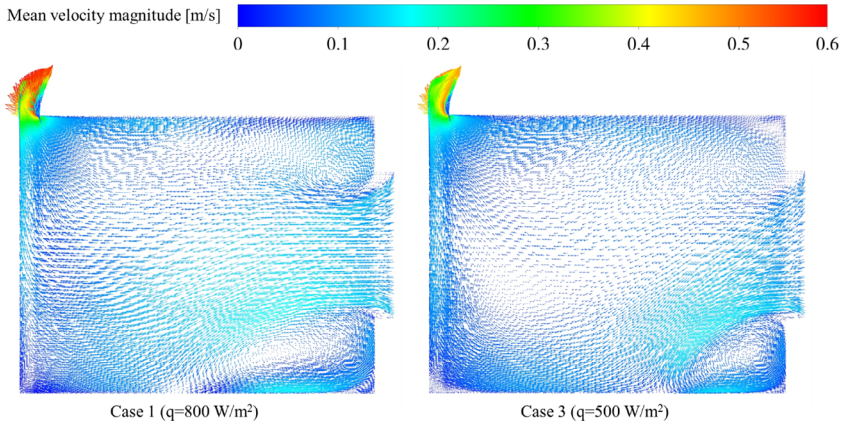

Fig. 11 Velocity vectors on the center plane of the room for Case 1 and Case 3

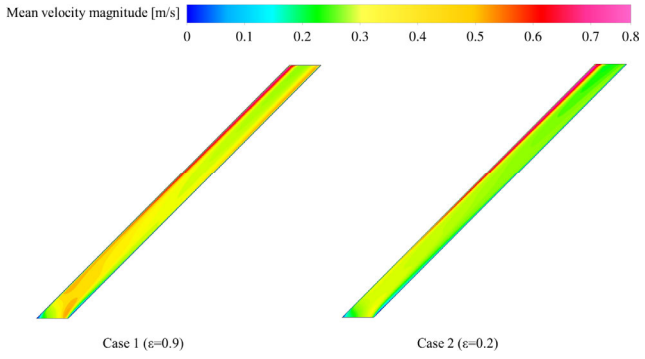

Fig. 12 Contours of mean velocity inside the channel on the center plane for Case 1 and Case 2

the roof surface when the emissivity is high or low. It is observed that the flow experiences higher velocities in the vicinity of the roof surface at higher surface emissivity than low emissivity. Consequently, the ventilation rate of the building and the passive cooling rate of the panels increase.

Contours of mean velocity vectors inside the building on the center plane are depicted in Figure 13 for the heat flux of 800 W/m^2 under different values for the roof surface emissivity (Case 1 and Case 2). It is observed that increasing the roof surface emissivity affects the flow structure inside the building. When the emissivity is high, due to the higher buoyant flow rate inside the channel, the momentum of flow entering the room from the window is higher than when the emissivity is low. Therefore, the inflow travels a longer path and touches the floor in the middle areas of the room resulting in the formation of a larger vortex. But, when the emissivity is low, due to lower flow momentum, the inflow touches the floor earlier yielding smaller vortexes.

4.4 Air change rate

A key parameter to evaluate the efficacy of ventilation in a confined space is the air change rate per hour (ACH) defined as:

$$\mathrm{ACH} = \frac{3600 \times Q}{V} \tag{9}$$

where Q [m^3/s] is the volumetric flow rate, and V [m^3] is the volume of the ventilated space.

To assess the ventilation rate using the PV panels, ACH is calculated for different cases and compared to *ACH* values recommended for various residential or non-residential buildings in Table 5 (Sherman 2004; Siva Reddy et al. 2012; Maghrabie et al. 2022). It is found that the ventilation rate provided by the BIPV system under different operating conditions is sufficient to satisfy the air change requirements for indoors with different applications.

A comparative review of the performance of solar chimneys from the literature and current system performance is provided in Table 6. It is seen that, for a wide range of operating conditions, the performance of the proposed BIPV system is similar to or greater than the performance of

Table 5 A comparison between the ACH obtained in this study with those recommended for various indoors

Indoor type	ACH
Bedrooms	2–4
Gathering halls	4–8
Lecture halls	5–8
libraries	3.5
Living rooms	3–6
Toilets	6–10
churches	1–3
Garages	6–8
offices	6–10
Schoolrooms	5–7
Banks	4–8
Stores and warehouses	3–6
Current study	3–13

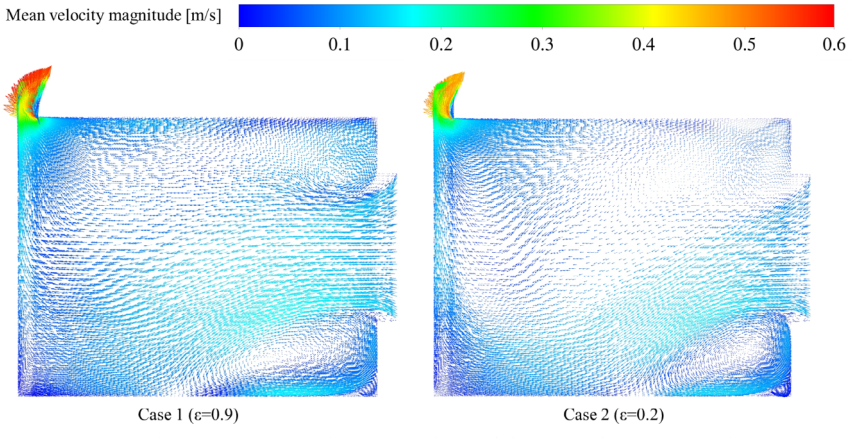

Fig. 13 Velocity vectors on the center plane of the room for Case 1 and Case 2

Table 6 Comparison of the performance of the current BIPV system with solar chimney systems from literature

Authors	Study type	Room dimensions [m]	Chimney or channel dimensions [m]	Applied heat flux [W/m^2]	Buoyancy-driven mass flow rate [kg/s]	ACH
Khanal and Lei (2015)	Numerical (2D)	Height: 3	Height: 2.5 Gap: 0.4	300–1000	—	8–15
Mathur et al. (2006)	Experimental	1 × 1 × 1	Height: 1 Width: 1 Gap: 0.1–0.3	300–700	—	2–5.6
Haghighi and Maerefat (2014)	Numerical (3D)	4 × 4 × 3.125	Height: 3.125 Width: 4 Gap: 0.2	50–600	—	2.21–8.69
Maerefat and Haghighi (2010)	Analytical	4 × 4 × 3.125	Height: 3.125 Width: 4 Gap: 0.2	200–1000	—	1.57–7.95
Huynh (2012)	Numerical (3D)	5 × 5 × 3	Height: 2 Width: 5 Gap: 0.2	0–800	0–0.52	—
Chen et al. (2003)	Experimental	—	Height: 1.5 Width: 0.62 Gap: 0.1–0.6	200–600	0.02–0.04	—
Imran et al. (2015)	Experimental and Numerical (3D)	2 × 3 × 2	Height: 2 Width: 2 Gap: 0.05–0.15	150–750	0.02–0.14	—
Liu et al. (2015)	Experimental	—	Height: 1 Width: 1 Gap: 0.1–0.6	120–958	0.022–0.19	—
Current study	Numerical (3D)	4 × 6 × 3	Height: 1.61 Width: 5.67 Gap: 0.15	200–800	0.065–0.306	3–13

studied solar chimneys in terms of *ACH* or buoyancy-driven mass flow rate used for passive ventilation and can provide efficient ventilation by supplying fresh air. On the other hand, the BIPV system offers the opportunity to generate electricity from solar radiation as a clean renewable energy resource while a conventional solar chimney system solely provides ventilation.

4.5 Efficiency and lifespan of the solar panels

The effects of overheating of solar panels are reflected in their electrical efficiency and lifespan. According to Evans (1981), the efficiency of a solar panel operating at a temperature above its standard testing condition (STC) could be estimated as:

$$\eta = \eta_{T_{STC}} [1 - \lambda_{STC} (T_{PV} - T_{STC}) + \gamma \log G] \quad (10)$$

where γ and λ_{STC} stand for efficiency correction coefficients for solar irradiance and temperature, respectively. Often, γ is considered zero (Evans and Florschuetz 1978) resulting in the following formulation:

$$\eta = \eta_{T_{STC}} [1 - \lambda_{STC} (T_{PV} - T_{STC})] \quad (11)$$

λ_{STC} can be approximated by (Wilson and Paul 2011):

$$\lambda_{STC} = \frac{1}{T_{\eta=0} - T_{STC}} \quad (12)$$

$T_{\eta=0}$ = 543 K represents the temperature at which the efficiency of the panel declines to zero (Evans and Florschuetz 1978).

From the manufacturer's datasheet, the other parameters are $\eta_{T_{STC}}$ = 20.6% and T_{STC} = 298 K.

Given the information above, a 3 K reduction in the mean temperature of the panels (corresponding to Case 1 compared with Case 2 due to increased roof surface emissivity) increases the efficiency of PV panels by about 1.56%.

According to Dupré et al. (2017) a 1 K decrease in the operating temperature of a PV panel could increase its lifespan by about 7% or two years. Therefore, it could be deduced that a 3 K decrease in the operating temperature of the panel due to enhanced roof surface emissivity would increase its lifespan by about 21%.

5 Conclusions and future perspectives

In the current study, a BIPV system has been proposed to assess its performance in terms of passive ventilation of a room and passive cooling of the rooftop-mounted PV panels.

For this purpose, a parametric study through 3D numerical modelling has been conducted. Different solar heat fluxes and ambient temperatures under the natural convection mechanism have been considered. Besides, the role of surface emissivity for the part of the roof beneath the PV panels has been evaluated. The main conclusions can be drawn from this investigation are:

- Under identical conditions, using the BIPV system instead of its counterpart BAPV system shows no adverse impact on the operating temperature of the PV panels. However, the proposed BIPV system provides the opportunity for passive ventilation of the building's interior.
- The performance of the proposed BIPV system in passive ventilation of buildings under different operating conditions is similar or slightly overperforms the common solar chimney systems used in the literature. But the BIPV system provides an opportunity to use solar energy as a renewable and clean energy resource for electricity generation.
- Increasing the surface emissivity for the part of the roof beneath the PV panels intensifies the natural convective currents which in turn provides better cooling for PV panels and higher passive ventilation rates for the indoors. Up to a 3 K decrease in the mean operating temperature of the panels and a 34% increase in the convective mass flow rate were observed by increasing the roof surface emissivity from 0.2 to 0.9 under different conditions. The cooling effects were prominent at higher heat flux.
- A 3 K decrease in the operating temperature of the solar panel can increase its efficiency and lifespan by about 1.56% and 21%, respectively.
- The flow structure inside the building is dependent on the applied heat flux and the roof surface emissivity. The inflow travels a longer path and generates larger vortexes at higher heat fluxes and higher surface emissivity due to the higher momentum of the flow under these conditions.

This research was conducted under natural convection conditions. However, further studies are required to assess the system's performance under wind conditions for a wide range of temperatures and heat fluxes to model a whole-day condition. Besides, it is of future research interests to investigate the system's performance when coupled with water evaporative cooling systems which are widely used in relatively warm and dry climates.

Acknowledgements

The financial support provided for the first author through the Australian Government Research Training Program (RTP) Scholarship is appreciated. The computations of this research were performed on the super-computer Gadi with the assistance of resources and services from the National Computational Infrastructure (NCI), which is supported by the Australian Government.

Funding note: Open Access funding enabled and organized by CAUL and its Member Institutions.

Declaration of competing interest

The authors have no competing interests to declare that are relevant to the content of this article.

Author contribution statement

H. Ahmadi Moghaddam: conceptualization, methodology, software, validation, formal analysis, investigation, writing—original draft, visualization. S. Tkachenko: software, review & editing. G.H. Yeoh: review & editing. V. Timchenko: conceptualization, review & editing, supervision.

References

Agathokleous RA, Kalogirou SA (2018a). Part I: Thermal analysis of naturally ventilated BIPV system: Experimental investigation and convective heat transfer coefficients estimation. *Solar Energy*, 169: 673–681.

Agathokleous RA, Kalogirou SA (2018b). Part II: thermal analysis of naturally ventilated BIPV system: Modeling and Simulation. *Solar Energy*, 169: 682–691.

Ahmed A, Ge T, Peng J, et al. (2022). Assessment of the renewable energy generation towards net-zero energy buildings: A review. *Energy and Buildings*, 256: 111755.

Alizadeh H, Ghasempour R, Shafii MB, et al. (2018). Numerical simulation of PV cooling by using single turn pulsating heat pipe. *International Journal of Heat and Mass Transfer*, 127: 203–208.

Ampofo F, Karayiannis TG (2003). Experimental benchmark data for turbulent natural convection in an air filled square cavity. *International Journal of Heat and Mass Transfer*, 46: 3551–3572.

An Y, Sheng C, Li X (2019). Radiative cooling of solar cells: Opto-electro-thermal physics and modeling. *Nanoscale*, 11: 17073–17083.

ANSYS (2021). Ansys Fluent, Release 2021 R1. Theory Guide. Canonsburg, PA, USA: ANSYS Inc.

Arifin Z, Tjahjana DDDP, Hadi S, et al. (2020). Numerical and experimental investigation of air cooling for photovoltaic panels using aluminum heat sinks. *International Journal of Photoenergy*, 2020: 1574274.

Asefi G, Habibollahzade A, Ma T, et al. (2021). Thermal management of building-integrated photovoltaic/thermal systems: A comprehensive review. *Solar Energy*, 216: 188–210.

Bansal NK, Mathur R, Bhandari MS (1993). Solar chimney for enhanced stack ventilation. *Building and Environment*, 28: 373–377.

Beji T, Zadeh SE, Maragkos G, et al. (2017). Influence of the particle injection rate, droplet size distribution and volume flux angular distribution on the results and computational time of water spray CFD simulations. *Fire Safety Journal*, 91: 586–595.

Brandl D, Mach T, Grobbauer M, et al. (2014). Analysis of ventilation effects and the thermal behaviour of multifunctional façade elements with 3D CFD models. *Energy and Buildings*, 85: 305–320.

Chen ZD, Bandopadhayay P, Halldorsson J, et al. (2003). An experimental investigation of a solar chimney model with uniform wall heat flux. *Building and Environment*, 38: 893–906.

Daghigh R, Ruslan MH, Sopian K (2011). Advances in liquid based photovoltaic/thermal (PV/T) collectors. *Renewable and Sustainable Energy Reviews*, 15: 4156–4170.

DeBlois JC, Bilec MM, Schaefer LA (2013). Design and zonal building energy modeling of a roof integrated solar chimney. *Renewable Energy*, 52: 241–250.

Dupré O, Vaillon R, Green MA (2017). Thermal Behavior of Photovoltaic Devices. Cham, Switzerland: Springer.

Dwivedi P, Sudhakar K, Soni A, et al. (2020). Advanced cooling techniques of P.V. modules: A state of art. *Case Studies in Thermal Engineering*, 21: 100674.

Elnozahy A, Rahman AKA, Ali AHH, et al. (2015). Performance of a PV module integrated with standalone building in hot arid areas as enhanced by surface cooling and cleaning. *Energy and Buildings*, 88: 100–109.

Evangelisti L, Guattari C, Asdrubali F (2019). On the sky temperature models and their influence on buildings energy performance: A critical review. *Energy and Buildings*, 183: 607–625.

Evans DL, Florschuetz LW (1978). Terrestrial concentrating photovoltaic power system studies. *Solar Energy*, 20: 37–43.

Evans DL (1981). Simplified method for predicting photovoltaic array output. *Solar Energy*, 27: 555–560.

Firoozzadeh M, Shiravi A, Shafiee M (2019). An experimental study on cooling the photovoltaic modules by fins to improve power generation: economic assessment. *Iranian (Iranica) Journal of Energy & Environment*, 10(2): 80–84.

Gan G (2009). Numerical determination of adequate air gaps for building-integrated photovoltaics. *Solar Energy*, 83: 1253–1273.

Habeeb LJ, Mutasher DG, Abd Ali FAM (2017). Cooling photovoltaic thermal solar panel by using heat pipe at Baghdad climate. *International Journal of Mechanical & Mechatronics Engineering*, 17(6): 171-185.

Haghighi AP, Maerefat M (2014). Solar ventilation and heating of buildings in sunny winter days using solar chimney. *Sustainable Cities and Society*, 10: 72–79.

Huynh BP (2012). Natural-ventilation flow in a 3-D room fitted with solar chimney. In: Proceedings of ASME 2012 International Mechanical Engineering Congress and Exposition, Houston, TX, USA.

Imran AA, Jalil JM, Ahmed ST (2015). Induced flow for ventilation and cooling by a solar chimney. *Renewable Energy*, 78: 236–244.

Jomehzadeh F, Nejat P, Calautit JK, et al. (2017). A review on windcatcher for passive cooling and natural ventilation in buildings, Part 1: indoor air quality and thermal comfort assessment. *Renewable and Sustainable Energy Reviews*, 70: 736–756.

Kabeel AE, Abdelgaied M, Sathyamurthy R (2019). A comprehensive investigation of the optimization cooling technique for improving the performance of PV module with reflectors under Egyptian conditions. *Solar Energy*, 186: 257–263.

Karthick A, Ramanan P, Ghosh A, et al. (2020). Performance enhancement of copper indium diselenide photovoltaic module using inorganic phase change material. *Asia-Pacific Journal of Chemical Engineering*, 15: e2480.

Khanal R, Lei C (2011). Solar chimney—A passive strategy for natural ventilation. *Energy and Buildings*, 43: 1811–1819.

Khanal R, Lei C (2015). A numerical investigation of buoyancy induced turbulent air flow in an inclined passive wall solar chimney for natural ventilation. *Energy and Buildings*, 93: 217–226.

Khedari J, Ingkawanich S, Waewsak J, et al. (2002). A PV system enhanced the performance of roof solar collector. *Building and Environment*, 37: 1317–1320.

Lai C, Hokoi S (2017). Experimental and numerical studies on the thermal performance of ventilated BIPV curtain walls. *Indoor and Built Environment*, 26: 1243–1256.

Lau GE, Yeoh GH, Timchenko V, et al. (2012a). Numerical investigation of passive cooling in open vertical channels. *Applied Thermal Engineering*, 39: 121–131.

Lau GE, Sanvicente E, Yeoh GH, et al. (2012b). Modelling of natural convection in vertical and tilted photovoltaic applications. *Energy and Buildings*, 55: 810–822.

Lau S-K, Zhao Y, Lau SSY, et al. (2020). An investigation on ventilation of building-integrated photovoltaics system using numerical modeling. *Journal of Solar Energy Engineering*, 142: 011016.

Li W, Yeoh GH, Timchenko V (2015). Large Eddy Simulation of turbulent buoyancy-driven flow with alternating staggered heating walls. *Applied Thermal Engineering*, 89: 558–568.

Liu B, Ma X, Wang X, et al. (2015). Experimental study of the chimney effect in a solar hybrid double wall. *Solar Energy*, 115: 1–9.

Maerefat M, Haghighi AP (2010). Natural cooling of stand-alone houses using solar chimney and evaporative cooling cavity. *Renewable Energy*, 35: 2040–2052.

Maghrabie HM, Mohamed ASA, Salem Ahmed M (2020). Experimental investigation of a combined photovoltaic thermal system via air cooling for summer weather of Egypt. *Journal of Thermal Science and Engineering Applications*, 12: 041022.

Maghrabie HM, Elsaid K, Sayed ET, et al. (2021). Building-integrated photovoltaic/thermal (BIPVT) systems: Applications and challenges. *Sustainable Energy Technologies and Assessments*, 45: 101151.

Maghrabie HM, Ali Abdelkareem M, Elsaid K, et al. (2022). A review of solar chimney for natural ventilation of residential and non-residential buildings. *Sustainable Energy Technologies and Assessments*, 52: 102082.

Mathur J, Bansal NK, Mathur S, et al. (2006). Experimental investigations on solar chimney for room ventilation. *Solar Energy*, 80: 927–935.

Mathur J, Mathur S (2006). Summer-performance of inclined roof solar chimney for natural ventilation. *Energy and Buildings*, 38: 1156–1163.

Menter FR (1994). Two-equation eddy-viscosity turbulence models for engineering applications. *AIAA Journal*, 32: 1598–1605.

Moharram KA, Abd-Elhady MS, Kandil HA, et al. (2013). Enhancing the performance of photovoltaic panels by water cooling. *Ain Shams Engineering Journal*, 4: 869–877.

Moghaddam HA, Shafaee M, Riazi R (2019). Numerical investigation of a refrigeration ejector: effects of environment-friendly refrigerants and geometry of the ejector mixing chamber. *European Journal of Sustainable Development Research*, 3: em0090.

Moosavi L, Zandi M, Bidi M, et al. (2020). New design for solar chimney with integrated windcatcher for space cooling and ventilation. *Building and Environment*, 181: 106785.

Orme M (2001). Estimates of the energy impact of ventilation and associated financial expenditures. *Energy and Buildings*, 33: 199–205.

Park D, Battaglia F (2015). Application of a wall-solar chimney for passive ventilation of dwellings. *Journal of Solar Energy Engineering*, 137: 061006.

Parkunam N, Pandiyan L, Navaneethakrishnan G, et al. (2020). Experimental analysis on passive cooling of flat photovoltaic panel with heat sink and wick structure. *Energy Sources, Part A: Recovery, Utilization, and Environmental Effects*, 42: 653–663.

Pérez-Lombard L, Ortiz J, Pout C (2008). A review on buildings energy consumption information. *Energy and Buildings*, 40: 394–398.

Prudhvi P, Sai PC (2012). Efficiency improvement of solar PV panels using active cooling. In: Proceedings of 2012 11th International Conference on Environment and Electrical Engineering, Venice, Italy.

Rabani R, Faghih AK, Rabani M, et al. (2014). Numerical simulation of an innovated building cooling system with combination of solar chimney and water spraying system. *Heat and Mass Transfer*, 50: 1609–1625.

Ritzen MJ, Vroon ZAEP, Rovers R, et al. (2017). Comparative performance assessment of a non-ventilated and ventilated BIPV rooftop configurations in the Netherlands. *Solar Energy*, 146: 389–400.

Sajjad U, Amer M, Ali HM, et al. (2019). Cost effective cooling of photovoltaic modules to improve efficiency. *Case Studies in Thermal Engineering*, 14: 100420.

Salem MR, Elsayed MM, Abd-Elaziz AA, et al. (2019). Performance enhancement of the photovoltaic cells using Al_2O_3/PCM mixture and/or water cooling-techniques. *Renewable Energy*, 138: 876–890.

Sartori I, Napolitano A, Voss K (2012). Net zero energy buildings: A consistent definition framework. *Energy and Buildings*, 48: 220–232.

Sherman MH (2004). ASHRAE's first residential ventilation standard. In: Proceedings of Buildings IX Conference, Clearwater, FL, USA.

Shukla AK, Sudhakar K, Baredar P (2017). Recent advancement in BIPV product technologies: A review. *Energy and Buildings*, 140: 188–195.

Singh D, Chaudhary R, Karthick A (2021). Review on the progress of building-applied/integrated photovoltaic system. *Environmental Science and Pollution Research*, 28: 47689–47724.

Siva Reddy V, Premalatha M, Ranjan KR (2012). Experimental studies on solar chimney for enhanced ventilation. *International Journal of Sustainable Energy*, 31: 35–42.

Sun X, Silverman TJ, Zhou Z, et al. (2017). Optics-based approach to thermal management of photovoltaics: selective-spectral and radiative cooling. *IEEE Journal of Photovoltaics*, 7: 566–574.

Swinbank WC (1963). Long-wave radiation from clear skies. *Quarterly Journal of the Royal Meteorological Society*, 89: 339–348.

Tian YS, Karayiannis TG (2000). Low turbulence natural convection in an air filled square cavity: part I: the thermal and fluid flow fields. *International Journal of Heat and Mass Transfer*, 43: 849–866.

Tkachenko OA, Timchenko V, Giroux-Julien S, et al. (2016). Numerical and experimental investigation of unsteady natural convection in a non-uniformly heated vertical open-ended channel. *International Journal of Thermal Sciences*, 99: 9–25.

Tkachenko SA, Moghaddam HA, Reizes JA, et al. (2021). Computational study of natural convection flow in an open-ended channel coupled with a room: Application to building-integrated photovoltaic (BIPV) systems. In: Proceedings of CHT-21 ICHMT International Symposium on Advances in Computational Heat Transfer, Rio de Janeiro, Brazil.

Wilson MJ, Paul MC (2011). Effect of mounting geometry on convection occurring under a photovoltaic panel and the corresponding efficiency using CFD. *Solar Energy*, 85: 2540–2550.

Wu T, Lei C (2015). On numerical modelling of conjugate turbulent natural convection and radiation in a differentially heated cavity. *International Journal of Heat and Mass Transfer*, 91: 454–466.

Zhai XQ, Dai YJ, Wang RZ (2005). Experimental investigation on air heating and natural ventilation of a solar air collector. *Energy and Buildings*, 37: 373–381.

Zhang R, Gan Y, Mirzaei PA (2020). A new regression model to predict BIPV cell temperature for various climates using a high-resolution CFD microclimate model. *Advances in Building Energy Research*, 14: 527–549.

Zhang H, Yang D, Tam VWY, et al. (2021). A critical review of combined natural ventilation techniques in sustainable buildings. *Renewable and Sustainable Energy Reviews*, 141: 110795.

Zhou Z, Jiang Y, Ekins-Daukes N, et al. (2021). Optical and thermal emission benefits of differently textured glass for photovoltaic modules. *IEEE Journal of Photovoltaics*, 11: 131–137.

Zhou Z, Tkachenko S, Bahl P, et al. (2022). Passive PV module cooling under free convection through vortex generators. *Renewable Energy*, 190: 319–329.